A simple and accurate discontinuous Galerkin scheme for modeling scalar-wave propagation in media with curved interfaces

Xiangxiong Zhang[1] *and Sirui Tan*[2]

ABSTRACT

Conventional high-order discontinuous Galerkin schemes suffer from interface errors caused by the misalignment between straight-sided elements and curved material interfaces. We develop a novel discontinuous Galerkin scheme to reduce the errors. Our new scheme use the correct normal vectors to the curved interfaces, while the conventional scheme uses the normal vectors to the element edge. We modify the numerical fluxes to account for the curved interface. Our numerical modeling examples demonstrate that our new discontinuous Galerkin scheme gives errors with much smaller magnitudes compared with the conventional scheme, although both schemes have second-order convergence. Moreover, our method significantly suppresses the spurious diffractions seen in the results obtained using the conventional scheme. The computational cost of our scheme is similar to that of the conventional scheme. Our new discontinuous Galerkin scheme is thus particularly useful for large-scale scalar-wave modeling involving complex subsurface structures.

INTRODUCTION

Discontinuous Galerkin (DG) finite element methods have been developed for a wide range of problems since their inception in the 1970's (e.g., Reed and Hill, 1973; Cockburn and Shu, 1989; Hesthaven and Warburton, 2007). In contrast to classical continuous finite element methods, the solution of DG methods can be discontinuous across element interfaces. The weak coupling between elements makes the mass matrix local to the cell, and thus DG schemes are compact since communication only with immediate neighbors is needed. DG methods are among attractive choices for handling complicated geometries and allowing hanging nodes in the mesh. DG methods have gained popularity for seismic modeling since the work of Käser and Dumbser (2006).

For simulations of waves propagating in piece-wise constant media, DG methods with an interface-fitting triangular mesh can capture material discontinuity more accurately than methods based on unstructured meshes. However, the errors caused by misalignment between straight-sided elements and curved interfaces remain an issue. When triangular meshes are used to fit curved boundaries, any continuous finite element method for elliptic equations is at most second-order accurate for the solution and 1.5-order accurate for the gradient of the solution (Strang and Berger, 1971; Thomée, 1973). DG methods using high-order polynomial bases for hyperbolic equations are at most second-order accurate for the solution (e.g., Bassi and Rebay, 1997). In the presence of curved material interfaces,

the same accuracy reduction holds for wave-propagation modeling if we assume homogeneous media on each element (Toulorge et al., 2008; Wang, 2010; Fahs, 2011). In seismic modeling, the interface errors may lead to spurious diffractions in the calculated wavefield, particularly when the element size is comparable to the wavelength. The wave energy of the spurious diffractions is much smaller than that of the primary reflections, but is comparable to that of the multiple reflections.

Although the overall error is dominated by the second-order interface error on fine meshes, choosing the order of the polynomial basis depends on the problem (e.g., model, data frequency spectrum, etc.), the available computational resources, and the desired modeling quality. For example, Käser and Dumbser (2006) developed arbitrary high-order polynomial bases, and used up to 10th-order polynomial for the Lamb's problem. Etienne et al. (2010) advocated low-order polynomial bases for very complex media. In general, very high-order polynomial bases are popular when a coarse mesh is used, because the dispersion error usually causes more harm than the interface error in seismic imaging and inversion. In fact, finite-difference methods with second-order accuracy in time and high-order accuracy in space are widely used, although the interface error is at most first order (Symes and Vdovina, 2009).

To reduce errors caused by curved geometries, curved elements have been developed (e.g., Monk and Wang, 1999; Barucq et al., 2014). For the optimal order of convergence, the standard approach is using curvilinear elements (Gordon and Hall, 1973) to represent curved interfaces. The curvilinear elements are constructed using isoparametric coordinate transforms. Every curvilinear element has its own mass matrix needed to be factored and stored, leading to prohibitive computer-memory requirement when a large number of curvilinear elements are used to fit complex interfaces. Although the computer-memory requirement is mitigated by the low-storage curvilinear DG method (Warburton, 2013), significant extra efforts are needed for implementation. In this paper, we aim to develop a simpler algorithm to reduce the interface errors.

Krivodonova and Berger (2006) introduced a simple way to approximate curvilinear boundaries and reduce the boundary errors for gas dynamics problems using the correct representation of the normal vectors to the interface geometry. This approach avoids the use of curvilinear elements. However, we observed from our numerical experiments that extending this approach to interface problems leads to almost the same results as the conventional DG scheme.

We present a simple correction to the DG methods on triangles to reduce errors due to piece-wise segment approximation of curved interfaces. We not only use the correct normal vectors to the curved interfaces, but also modify the numerical fluxes evaluation points. We demonstrate the effectiveness of our simple correction using numerical modeling of scalar-wave propagation in media with curved interfaces. Our examples demonstrate that our new DG scheme gives errors with much smaller magnitudes compared with the conventional DG scheme, although both schemes have second-order convergence. Our method is certainly not as accurate as curvilinear elements, but the advantage of our method is its simplicity, especially for problems involving multiple complex interfaces.

DISCONTINUOUS GALERKIN METHODS

Let $\mathbf{x} = (x, z)$ denote the spatial variables. The scalar-wave equation for pressure p and velocity $\mathbf{v} = (v_x, v_z)$ is given by

$$\begin{aligned} \rho(\mathbf{x})\frac{\partial \mathbf{v}}{\partial t} + \nabla p &= \mathbf{0}, \\ \frac{1}{\kappa(\mathbf{x})}p_t + \nabla \cdot \mathbf{v} &= s(\mathbf{x}, t), \end{aligned} \tag{1}$$

where ρ is density and κ is bulk modulus. We only consider models composed of piece-wise constant media. The wave speed is $c = \sqrt{\kappa/\rho}$. The point source is given by $s(\mathbf{x}, t) = f(t)\delta(\mathbf{x} - \mathbf{x}_s)$, where $\mathbf{x}_s$ is the source location and $f(t)$ is the source time function. We can rewrite equation 1 as

$$\mathbf{w}_t + \mathbf{A}(x, z)\mathbf{w}_x + \mathbf{B}(x, z)\mathbf{w}_z = [0, 0, \kappa f(t)\delta(\mathbf{x} - \mathbf{x}_s)]^T, \tag{2}$$

where $\mathbf{w} = [v_x, v_z, p]^T$ and

$$\mathbf{A} = \begin{pmatrix} 0 & 0 & 1/\rho \\ 0 & 0 & 0 \\ \kappa & 0 & 0 \end{pmatrix}, \quad \mathbf{B} = \begin{pmatrix} 0 & 0 & 0 \\ 0 & 0 & 1/\rho \\ 0 & \kappa & 0 \end{pmatrix}. \tag{3}$$

For an interface-fitting triangular mesh, we set ρ and κ as constants on each triangle K. Multiplying equation 2 by a smooth test function u compactly supported in K and taking an integral over K, after integration by parts, we obtain

$$\int_K \mathbf{w}_t u \, dV - \int_K \left(\frac{\partial u}{\partial x}\mathbf{A} + \frac{\partial u}{\partial z}\mathbf{B}\right)\mathbf{w} \, dV + \int_{\partial K} u\mathbf{F} \, ds = \mathbf{s}(t)u(\mathbf{x}_s), \tag{4}$$

where $\mathbf{s}(t) = [0, 0, \kappa(\mathbf{x}_s)f(t)]^T$, the flux $\mathbf{F} = (n_x\mathbf{A} + n_z\mathbf{B})\mathbf{w}$, and $\mathbf{n} = (n_x, n_z)$ is the outward unit normal vector to the boundary ∂K of the triangle.

In DG methods, we seek piece-wise polynomials $\mathbf{w}_h$ satisfying the following weak formulation for any piece-wise polynomial test function u_h:

$$\frac{d}{dt}\int_K \mathbf{w}_h u_h \, dV - \int_K \left(\frac{\partial u_h}{\partial x}\mathbf{A} + \frac{\partial u_h}{\partial z}\mathbf{B}\right)\mathbf{w}_h \, dV + \int_{\partial K} u_h\hat{\mathbf{F}} ds = \mathbf{s}(t)u_h(\mathbf{x}_s), \tag{5}$$

where the numerical flux $\hat{\mathbf{F}} = (n_x\mathbf{A} + n_z\mathbf{B})\mathbf{w}^*$. Here $\mathbf{w}^*$ is an approximation to the values of $\mathbf{w}$ on the boundary, since $\mathbf{w}_h$ is discontinuous across the boundary ∂K. For instance, $\mathbf{w}^*$ can be taken as the exact solution of the 1D Riemann problem in the direction normal to each edge of K (Wang, 2010). We denote the three edges of K by e_K^i, $i = 1, 2, 3$, with outward unit normal vector $\mathbf{n}^i$. Let K_i denote the neighboring triangle along e_K^i and $\mathbf{w}_K$ denote the polynomial defined on K. Then the numerical flux term $\int_{\partial K} u_h\hat{\mathbf{F}} ds$ can be written as

$$\int_{\partial K} u_h\hat{\mathbf{F}} ds = \sum_{i=1}^{3}\int_{e_K^i} u_h\hat{\mathbf{F}} ds = \sum_{i=1}^{3}\int_{e_K^i} u_h(n_x^i\mathbf{A} + n_z^i\mathbf{B})\mathbf{w}^*[\mathbf{w}^{int(K)}, \mathbf{w}^{ext(K)}, \mathbf{n}^i] \, ds, \tag{6}$$

where $\mathbf{w}^{int(K)} = \mathbf{w}_K$ and $\mathbf{w}^{ext(K)} = \mathbf{w}_{K_i}$ for each edge e_K^i are the approximation values from inside and outside of K, respectively. For each edge e_K^i, let $v^{int(K)} = \mathbf{v}^{int(K)} \cdot \mathbf{n}^i$ and

$v^{ext(K)} = \mathbf{v}^{ext(K)} \cdot \mathbf{n}^i$ denote the normal velocities, then $\mathbf{w}^*[\mathbf{w}^{int(K)}, \mathbf{w}^{ext(K)}, \mathbf{n}^i]$ denotes the exact solution of the following 1D Riemann problem:

$$\begin{aligned} &\rho(\xi)\frac{\partial v}{\partial t} + p_\xi = 0, \quad \frac{1}{\kappa(\xi)}p_t + v_\xi = 0, \\ &(v(\xi,0), p(\xi,0)) = \begin{cases} (v^{int(K)}, p^{int(K)}), & \xi < 0 \\ (v^{ext(K)}, p^{ext(K)}), & \xi > 0 \end{cases}, \\ &(\rho, \kappa) = \begin{cases} (\rho_K, \kappa_K), & \xi < 0 \\ (\rho_{K_i}, \kappa_{K_i}), & \xi > 0 \end{cases}. \end{aligned} \tag{7}$$

Applying integration by parts to equation 5, we obtain the equivalent strong formulation of the DG scheme:

$$\int_K \left(\frac{\partial \mathbf{w}_h}{\partial t} + \mathbf{A}\frac{\partial \mathbf{w}_h}{\partial x} + \mathbf{B}\frac{\partial \mathbf{w}_h}{\partial z} \right) u_h \, dV + \sum_{i=1}^{3} \int_{e_K^i} u_h(\hat{\mathbf{F}} - \mathbf{F}) ds = \mathbf{s}(t) u_h(\mathbf{x}_s). \tag{8}$$

The time evolution is solved by the fourth-order low-storage Runge-Kutta method (Hesthaven and Warburton, 2007).

A SIMPLE ACCURATE INTERFACE TREATMENT

We assume edge e_K^1 of triangle K approximates the curved interface, see Figure 1a for an illustration. We briefly review how to compute flux terms before introducing a simple geometrical correction to the flux term $\int_{e_K^1} u_h(\hat{\mathbf{F}} - \mathbf{F}) ds$ on this edge in equation 8. For convenience, we denote the integrand $u_h(\hat{\mathbf{F}} - \mathbf{F})$ as a function of $\mathbf{x} \in e_K^1$:

$$\mathbf{G}(\mathbf{x}, \mathbf{n}^1) = u_h(\mathbf{x})(n_x^1 \mathbf{A}_K + n_z^1 \mathbf{B}_K)(\mathbf{w}^*[\mathbf{w}_K(\mathbf{x}), \mathbf{w}_{K_1}(\mathbf{x}), \mathbf{n}^1] - \mathbf{w}_K(\mathbf{x})). \tag{9}$$

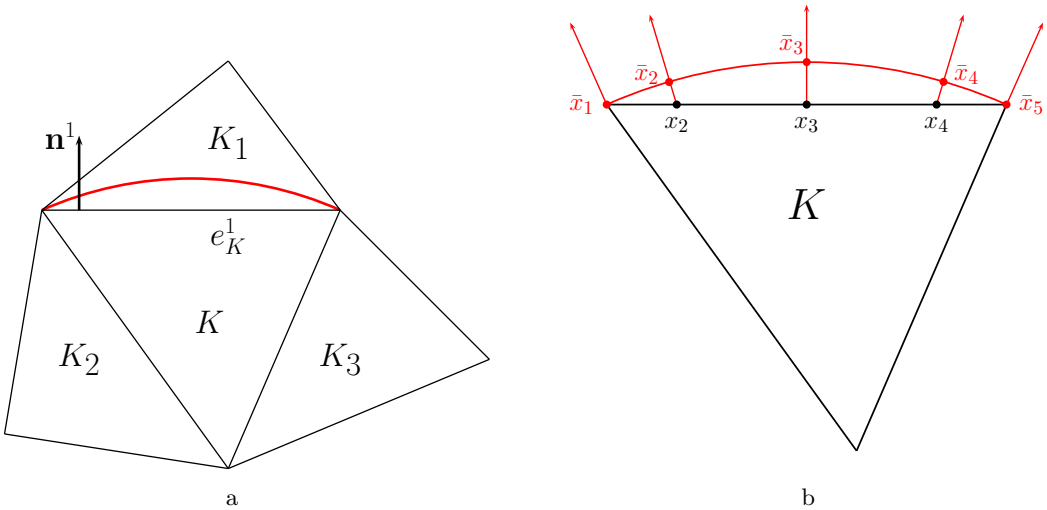

Figure 1: An illustration of (a) an element near the curved interface and (b) the projection of the quadrature points to the interface. The red curve is the material interface.

The line integral is computed by quadratures. We assume the polynomial degree of $\mathbf{w}_h$ is N, and we use the α-optimized nodal distribution points of triangle K to represent degrees of freedoms of all polynomials as discussed in Hesthaven and Warburton (2007). Then the line integral can be written as

$$\int_{e_K^1} u_h(\hat{\mathbf{F}} - \mathbf{F})ds = \sum_{j=1}^{N+1} \mathbf{G}(\mathbf{x}_j, \mathbf{n}^1)\omega_j, \tag{10}$$

where $\mathbf{x}_j$ $(j = 1, \cdots, N+1)$ are the nodal points of K lying on edge e_K^1, and ω_j denotes the corresponding weight with $\sum_{j=1}^{N+1} \omega_j$ equal to the length of the edge e_K^1.

We observe the following geometrical corrections to equation 10 reduce interface errors:

1. Find the projection points of $\mathbf{x}_j$ on the curve, denoted as $\bar{\mathbf{x}}_j$. See Figure 1b for an illustration.

2. Find a vector normal to the curve at the projection points $\bar{\mathbf{x}}_j$. For instance, we can use $\bar{\mathbf{x}}_j - \mathbf{x}_j$. The outward unit normal vector is denoted by $\mathbf{n}(\bar{\mathbf{x}}_j)$.

3. Replace $\mathbf{G}(\mathbf{x}_j, \mathbf{n}^1)$ by $\mathbf{G}(\bar{\mathbf{x}}_j, \mathbf{n}(\bar{\mathbf{x}}_j))$ in equation 10, i.e.,

$$\int_{e_K^1} u_h(\hat{\mathbf{F}} - \mathbf{F})ds = \sum_{j=1}^{N+1} \mathbf{G}(\bar{\mathbf{x}}_j, \mathbf{n}(\bar{\mathbf{x}}_j))\omega_j. \tag{11}$$

Let Γ denote the curve in Figure 1a. In the last step of this correction, notice that $\sum_{j=1}^{N+1} \mathbf{G}(\bar{\mathbf{x}}_j, \mathbf{n}(\bar{\mathbf{x}}_j))\omega_j$ in equation 11 is not a high-order accurate approximation of the integral $\int_\Gamma u_h(\hat{\mathbf{F}} - \mathbf{F})ds = \int_\Gamma \mathbf{G}(\mathbf{x}, \mathbf{n})ds$, because the arc length of the curve Γ is not included. Intuitively, the correction would be more accurate if we replaced $\int_{e_K^1} u_h(\hat{\mathbf{F}} - \mathbf{F})ds$ in equation 11 with an accurate approximation of $\int_\Gamma u_h(\hat{\mathbf{F}} - \mathbf{F})ds$. However, the function $(\hat{\mathbf{F}} - \mathbf{F})$ becomes zero on the interface curve Γ if $\mathbf{w}_K$ and $\mathbf{w}_{K_1}$ are equal to the exact solution in equation 9. Thus, $\int_\Gamma u_h(\hat{\mathbf{F}} - \mathbf{F})ds$ can be regarded as a penalty term approximating zero. When replacing the numerical solution $\mathbf{w}_K$ and $\mathbf{w}_{K_1}$ with the exact solution in equation 9, $\sum_{j=1}^{N+1} \mathbf{G}(\bar{\mathbf{x}}_j, \mathbf{n}(\bar{\mathbf{x}}_j))\omega_j$ in equation 11 is also zero, but $\int_{e_K^1} u_h(\hat{\mathbf{F}} - \mathbf{F})ds$ is second-order away from zero. Thus, $\sum_{j=1}^{N+1} \mathbf{G}(\bar{\mathbf{x}}_j, \mathbf{n}(\bar{\mathbf{x}}_j))\omega_j$ is a good approximation to the penalty term $\int_\Gamma u_h(\hat{\mathbf{F}} - \mathbf{F})ds$ from the point of view of the local truncation error, which explains why this correction may reduce interface errors. In our numerical tests, we did not observe any meaningful improvement by including the arc length in equation 11. Therefore, we recommend using the simple correction without involving the arc length.

We apply this correction for all edges approximating the curve. Our correction strategy is different from the one in Krivodonova and Berger (2006). Their method is developed for the solid wall boundary condition in gas dynamics problems. To extend the method to interface

problems, one may replace the normal vector in the flux term $\int_{e_K^i} u_h \hat{\mathbf{F}} ds$ in equation 6 with the correct normal vector to the interface geometry. However, our numerical tests suggest that such correction may not be consistent with the wave equation. A consistent correction is using the correct normal vector in the term $\int_{e_K^i} u_h(\hat{\mathbf{F}} - \mathbf{F}) ds$ in equation 8. Our numerical tests show that this correction hardly changes the modeling results obtained using the conventional DG scheme.

For highly curved interfaces, we have to locally refine the mesh such that the mesh size is sufficiently smaller than the radius of curvature. When the mesh size approaches zero, we obtain the asymptotic convergence rate of second order. For a given radius of curvature, it is very difficult to quantitatively analyze the maximum allowed mesh size for numerical stability and accuracy. Such analyses are out of the scope of this paper.

NUMERICAL EXAMPLES

We compare the accuracy of our simple geometrical correction with that of the conventional DG scheme. We do not show the results obtained using the method of Krivodonova and Berger (2006), because they are almost the same as those of the conventional DG scheme in all our numerical examples. In the first set of examples, the maximum errors of both methods are exactly the same within three significant figures. In the second set of examples, there is no visible difference between the common-shot gathers obtained using both methods.

Media with circular interfaces

We consider scattering of a plane wave by a cylinder with given analytical solution to test the accuracy of the geometrical correction. The cylinder is assumed to have a radius of $r_0 = 0.6$. Outside the cylinder, i.e., $\sqrt{x^2 + z^2} = r < r_0$, the density is constant ρ_1 and the bulk modulus is constant κ_1. For $r \geq r_0$, the density and bulk modulus are constants ρ_2 and κ_2, respectively. The source term $s(\mathbf{x}, t) = 0$ in equation 1. Assume the cylinder is illuminated by a plane wave of the form

$$p^{inc} = \exp\left(-\mathrm{i}(k_1 x - \omega t)\right), \quad u^{inc} = \exp\left(-\mathrm{i}(k_1 x - \omega t)\right), \quad v^{inc} = 0, \tag{12}$$

where $k_1 = \omega\sqrt{\rho_1/\kappa_1}$. Then the problem has an exact solution given as follows (Cai and Deng, 2003):

$$p(x, z, t) = p(r, \theta, t) = e^{\mathrm{i}\omega t} \begin{cases} \sum_{n=-\infty}^{\infty} C_n^{tot} J_n(k_2 r) e^{\mathrm{i}n\theta}, & r \leq r_0 \\ \sum_{n=-\infty}^{\infty} (\mathrm{i}^{-n} J_n(k_1 r) + C_n^{scat} H_n(k_1 r)) e^{\mathrm{i}n\theta}, & r > r_0 \end{cases}, \tag{13}$$

where $(r, \theta) = (\sqrt{x^2 + z^2}, \arctan(z/x))$ represent the polar coordinates, J_n and H_n represent the nth order Bessel function of the first kind and the Hankel function of the second kind, respectively, and $k_2 = \omega\sqrt{\rho_2/\kappa_2}$. The expansion coefficients are given as

$$C_n^{tot} = \mathrm{i}^{-n} \frac{\frac{k_1}{\rho_1} J_n'(k_1 r_0) H_n(k_1 r_0) - \frac{k_1}{\rho_1} H_n'(k_1 r_0) J_n(k_1 r_0)}{\frac{k_2}{\rho_2} J_n'(k_2 r_0) H_n(k_1 r_0) - \frac{k_1}{\rho_1} H_n'(k_1 r_0) J_n(k_2 r_0)}, \tag{14}$$

and

$$C_n^{scat} = \mathrm{i}^{-n} \frac{\frac{k_1}{\rho_1} J_n'(k_1 r_0) J_n(k_2 r_0) - \frac{k_2}{\rho_2} J_n'(k_2 r_0) J_n(k_1 r_0)}{\frac{k_2}{\rho_2} J_n'(k_2 r_0) H_n(k_1 r_0) - \frac{k_1}{\rho_1} H_n'(k_1 r_0) J_n(k_2 r_0)}. \tag{15}$$

Plug the pressure into equation 1, then we can obtain the expressions for the velocity.

The computational domain is $[-1.5, 1.5] \times [-1.5, 1.5]$ and we use PML of width 0.25 to terminate the computation at the boundaries. We set $\omega = 2\pi$ and use the real part the analytical solution to test the accuracy of DG schemes. The final time is set as $T = 0.4$ and we monitor the maximum error over the nodal points of each triangle inside the square $[-0.8, 0.8] \times [-0.8, 0.8]$ to exclude possible errors due to the PML. Mesh1 and Mesh2 used in the numerical tests are shown in Figure 2. Mesh3 is a straightforward refinement of Mesh2. We consider two cases with different velocity contrasts. One is with $\rho_1 = \kappa_1 = \rho_2 = 1$ and $\kappa_2 = 1/2.25$ such that the velocity contrast is $1 : 1.5$. We take $\rho_1 = \kappa_1 = \rho_2 = 1$ and $\kappa_2 = 1/25$ for the other case such that the velocity contrast is $1 : 5$.

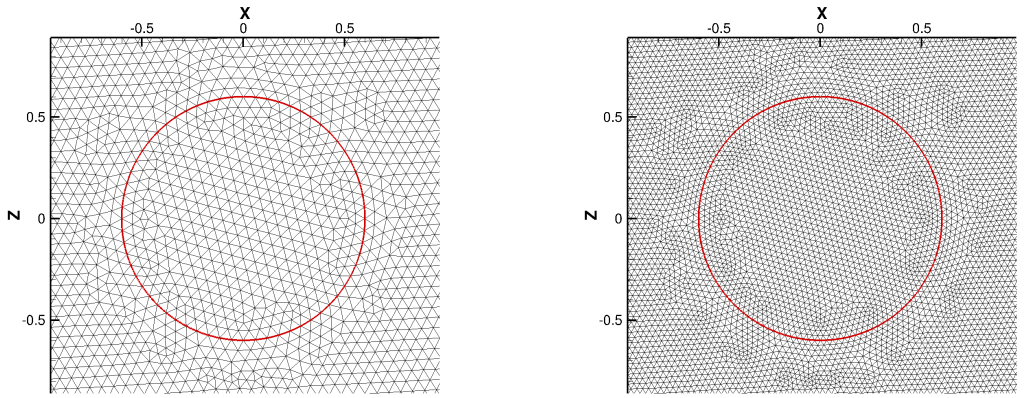

a b

Figure 2: (a) Mesh1 and (b) Mesh2 for DG modeling. Both meshes fit the circular material interface indicated by red lines.

The errors for the low contrast case are listed in Table 1 and the errors for the high contrast case are listed in Table 2. In Table 1, the error of the conventional DG scheme decreases significantly when the order of the polynomial basis is increased from $N = 2$ to $N = 3$ on Mesh1. When the order of the polynomial basis is further increased, the overall errors are almost unchanged on Mesh1. This is because the interface error dominates, and the conventional high-order DG scheme is not able to reduce the interface error without grid refinement. We can see that the simple geometrical correction reduces the error magnitude in both Tables 1 and 2. Even though there is an apparent reduction of the order of convergence for Mesh2 in the low contrast case, the convergence rate for the further refined Mesh3 is approximately second order for both DG schemes with polynomials of degree $N \geq 2$.

For comparison, we list the errors of the curvilinear element method in Table 3. In general, the curvilinear element method gives smaller errors and faster convergence rates than our modified DG method. However, in some cases, the errors of the two methods are similar. For example, in the case of velocity contrast $1 : 1.5$, the error of our method with the polynomial of degree $N = 2$ is 3.57E-3 on Mesh1, while the error of the curvilinear element method with the same N is 3.37E-3 on Mesh1. In the case of velocity contrast $1 : 5$, the errors of our method with polynomials of degrees $N = 2$ and $N = 3$ are almost

the same as those of the curvilinear element method with the same mesh. Thus, for some problems and certain given error thresholds, the performance of our DG method is similar to that of the curvilinear element method.

	Conventional DG					Modified DG				
N	Mesh1	Mesh2	order	Mesh3	order	Mesh1	Mesh2	order	Mesh3	order
2	7.13E-3	1.41E-3	2.33	3.03E-4	2.22	3.57E-3	4.78E-4	2.89	6.64E-5	2.85
3	4.11E-3	1.03E-3	1.99	2.58E-4	2.00	4.57E-4	9.94E-5	2.20	2.27E-5	2.13
4	4.11E-3	1.03E-3	2.00	2.58E-4	2.00	3.30E-4	8.36E-5	1.98	1.94E-5	2.11
5	4.12E-3	1.03E-3	2.00	2.58E-4	2.00	2.59E-4	7.02E-5	1.88	1.75E-5	2.00
6	4.12E-3	1.03E-3	2.00	2.58E-4	2.00	2.34E-4	6.38E-5	1.88	1.59E-5	2.00
7	4.13E-3	1.03E-3	2.00	2.58E-4	2.00	2.01E-4	5.66E-5	1.83	1.43E-5	1.98

Table 1: Errors for DG schemes with polynomials of degree N. The interface geometry is a circle, and the velocity contrast is $1 : 1.5$. Our new DG scheme gives errors with much smaller magnitudes compared with the conventional DG scheme, although both schemes have second-order convergence.

	Conventional DG					Modified DG				
N	Mesh1	Mesh2	order	Mesh3	order	Mesh1	Mesh2	order	Mesh3	order
2	1.12E-1	1.42E-2	2.98	2.39E-3	2.57	1.01E-1	1.18E-2	3.09	1.65E-3	2.84
3	2.38E-2	4.03E-3	2.56	9.98E-4	2.01	1.51E-2	1.05E-3	3.84	2.48E-4	2.08
4	1.62E-2	3.98E-3	2.02	9.95E-4	2.00	3.88E-3	8.81E-4	2.14	2.24E-4	1.97
5	1.62E-2	3.98E-3	2.02	9.96E-4	2.00	3.24E-3	8.03E-4	2.01	1.95E-4	2.04
6	1.62E-2	3.98E-3	2.02	9.96E-4	2.00	2.70E-3	6.93E-4	1.96	1.83E-4	1.92
7	1.62E-2	3.98E-3	2.03	9.96E-4	2.00	2.40E-3	6.23E-4	1.95	1.67E-4	1.90

Table 2: Errors for DG schemes with polynomials of degree N. The interface geometry is a circle, and the velocity contrast is $1 : 5$. Our new DG scheme gives much smaller errors than the conventional DG scheme.

Dome model

We consider a 2D dome model illustrated in Figure 3a where the density is constant everywhere. It is similar to the one used by Wang (2010). A Ricker-wavelet source with a central frequency of 25 Hz is located at (3300 m, 40 m). All 400 receivers lie uniformly on the line from (2300 m, 40 m) to (4300 m, 40 m).

We test DG methods with polynomial of degree 8 on the mesh shown in Figure 3b. This high polynomial order is necessary to ensure that there is no visible dispersion error in the modeled wavefields. Along the curved interface, the length of the edges of the triangles ranges from 35 m to 42 m, which is around the minimum wavelength. The conventional DG scheme on triangles produce spurious diffractions on this relatively coarse mesh due to the piece-wise segment approximation to the curve. In Figure 4a, we observe nonphysical scattering generated near the curved interface. We then apply the simple geometrical correction to the conventional DG scheme. The numerical diffractions are significantly suppressed

	Velocity contrast 1 : 1.5					Velocity contrast 1 : 5				
N	Mesh1	Mesh2	order	Mesh3	order	Mesh1	Mesh2	order	Mesh3	order
2	3.37E-3	4.72E-4	2.99	5.96E-5	2.99	9.99E-2	1.18E-2	3.07	1.65E-3	2.84
3	1.88E-4	1.37E-5	3.78	8.88E-7	3.95	1.51E-2	1.00E-3	3.91	6.84E-5	3.87
4	7.02E-6	2.24E-7	4.97	7.03E-9	4.99	1.95E-3	5.92E-5	5.04	2.08E-6	4.83
5	1.68E-7	3.41E-9	5.62	5.60E-11	5.93	1.61E-4	2.99E-6	5.75	5.09E-8	5.88
6	1.54E-7	3.70E-11	12.01	8.95E-13	5.37	1.62E-5	1.30E-7	6.96	1.13E-9	6.85
7	1.22E-7	1.44E-11	13.04	6.84E-14	7.72	9.54E-7	4.26E-9	7.80	1.83E-11	7.86

Table 3: Errors for DG schemes using curvilinear elements with polynomials of degree N. The interface geometry is a circle. In general, the curvilinear element method gives smaller errors and faster convergence rates than our modified DG method. However, in some cases, the errors of the two methods are similar.

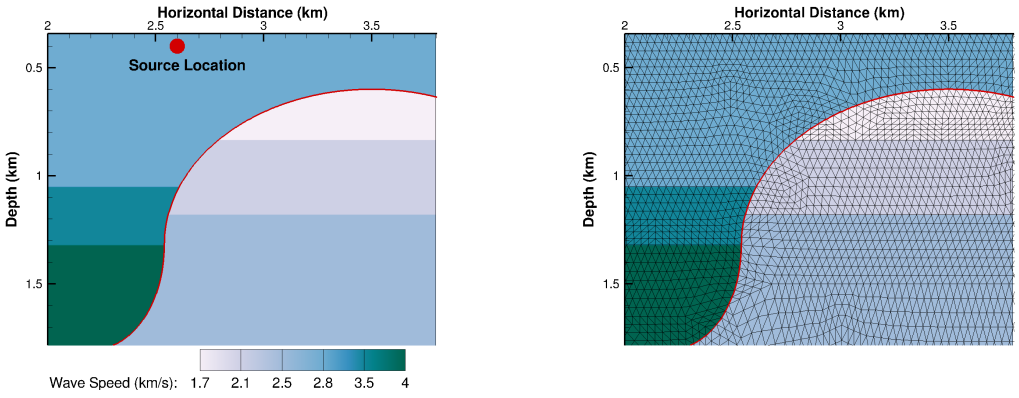

a b

Figure 3: (a) A 2D dome model; (b) the interface-fitting triangular mesh used for modeling.

(Figure 4b). The spurious diffractions generated by the conventional DG scheme also appear in the common-shot gather shown in Figure 5a. The spurious diffractions are almost invisible in the common-shot gather obtained using our geometrical correction (Figure 5b). Figure 6 displays traces obtained using both schemes at the receiver with an offset of 250 m. The reference trace is obtained using the conventional DG scheme with polynomial of degree 9 on a refined mesh. The trace obtained using our geometrical correction matches well with the reference one, while the conventional DG scheme gives spurious oscillations. The computational cost of our scheme is much smaller than that of the conventional DG scheme on the refined mesh.

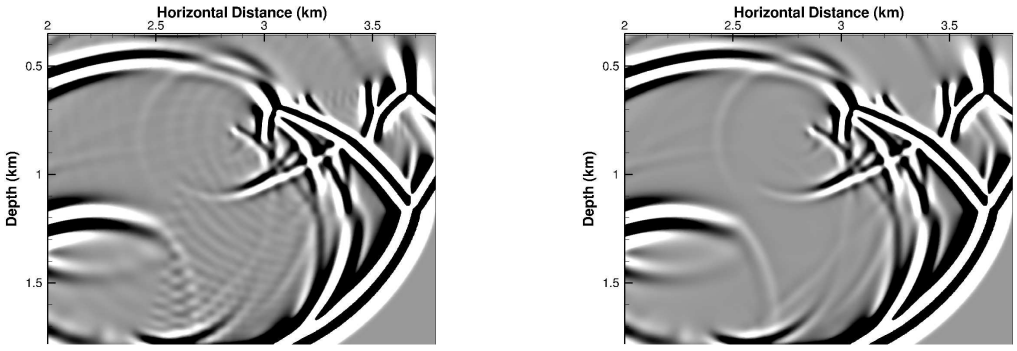

a b

Figure 4: Snapshots of the pressure wavefield at $T = 0.7$ s obtained using (a) the conventional DG scheme and (b) our DG scheme with simple geometrical correction. The snapshot in panel (a) contains spurious diffractions caused by interface error. Our geometrical correction significantly suppresses the spurious diffractions in panel (b).

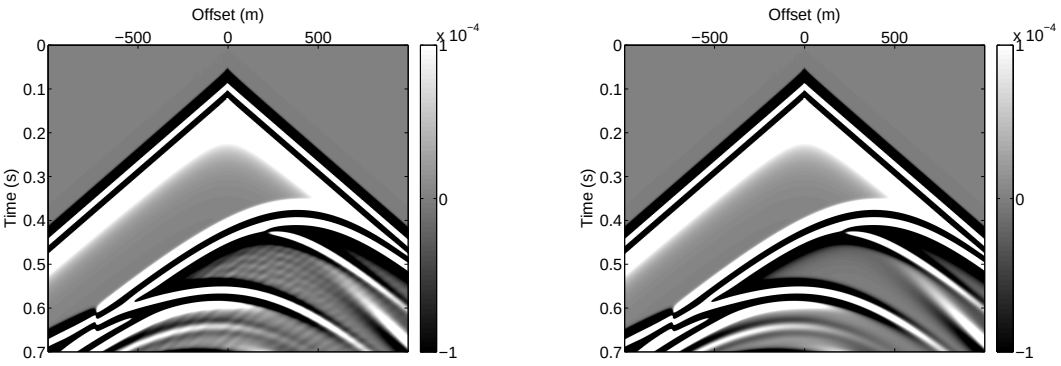

a b

Figure 5: Common-shot gather obtained using (a) the conventional DG scheme and (b) our DG scheme with simple geometrical correction. The spurious diffractions in panel (a) are almost invisible in panel (b).

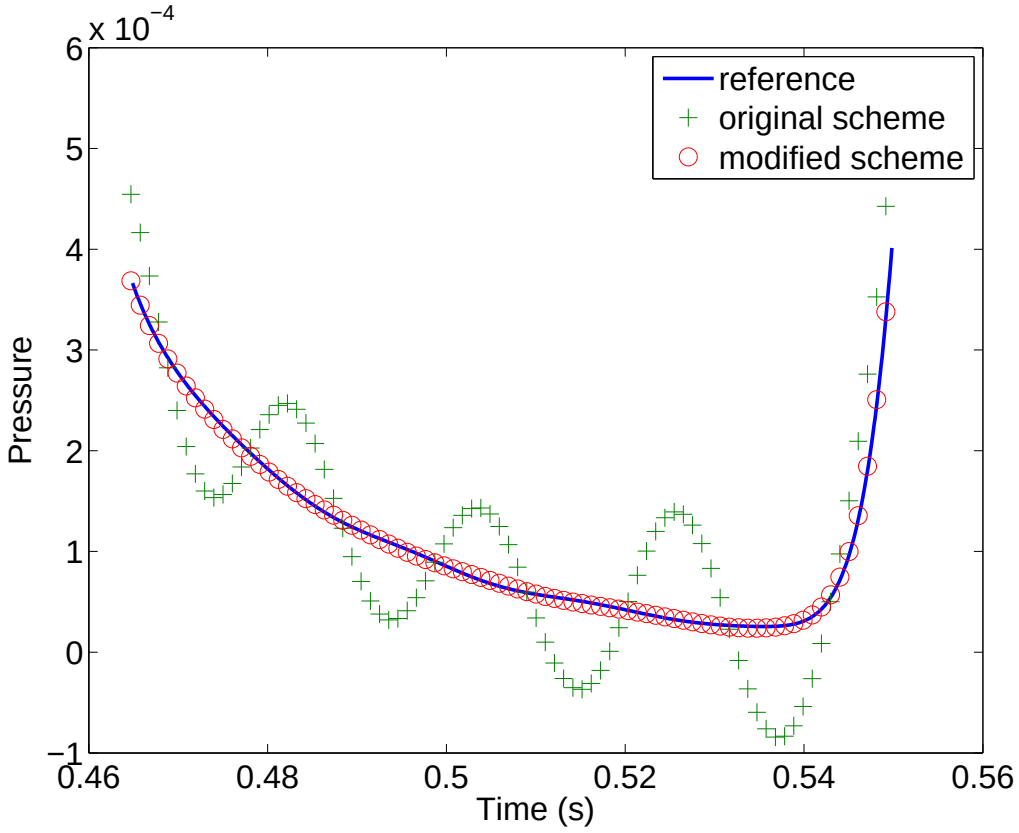

Figure 6: Traces obtained using the conventional DG scheme (green symbols) and our DG scheme (red symbols) at the receiver with an offset of 250 m. The blue curve shows the reference trace. The trace obtained using our DG scheme matches well with the reference one, while the conventional DG scheme gives spurious oscillations.

CONCLUSIONS

We have developed a novel discontinuous Galerkin scheme for modeling scalar-wave propagation in media with curved interfaces. As the conventional discontinuous Galerkin scheme, our scheme is based on straight-sided triangular elements. To account for curved interfaces, we use the correct normal vectors and modify the numerical fluxes. Numerical examples demonstrate that our new discontinuous Galerkin scheme gives much smaller errors compared with the conventional scheme, although both schemes have second-order convergence. For the dome model, the conventional scheme generates spurious diffractions caused by interface errors, while our scheme significantly suppresses the spurious diffractions. Our scheme gives a wavefield similar to that obtained using the conventional scheme on a refined mesh, but with a much smaller computational cost than the latter. Our new discontinuous Galerkin scheme is thus particularly useful for large-scale scalar-wave modeling involving complex subsurface structures.

ACKNOWLEDGMENTS

The work of Sirui Tan was supported by U.S. Department of Energy through contract DE-AC52-06NA25396 to Los Alamos National Laboratory. We thank Associate Editor and two anonymous reviewers for their valuable comments.

REFERENCES

Barucq, H., R. Djellouli, and E. Estecahandy, 2014, Efficient DG-like formulation equipped with curved boundary edges for solving elasto-acoustic scattering problems: International Journal for Numerical Methods in Engineering, **98**, 747–780.

Bassi, F., and S. Rebay, 1997, High-order accurate discontinuous finite element solution of the 2D Euler equations: Journal of computational physics, **138**, 251–285.

Cai, W., and S. Deng, 2003, An upwinding embedded boundary method for Maxwell's equations in media with material interfaces: 2D case: Journal of Computational Physics, **190**, 159–183.

Cockburn, B., and C.-W. Shu, 1989, TVB Runge-Kutta local projection discontinuous Galerkin finite element method for conservation laws II: General framework: Mathematics of Computation, **52**, pp. 411–435.

Etienne, V., E. Chaljub, J. Virieux, and N. Glinsky, 2010, An hp-adaptive discontinuous Galerkin finite-element method for 3-D elastic wave modelling: Geophysical Journal International, **183**, 941–962.

Fahs, H., 2011, Improving accuracy of high-order discontinuous Galerkin method for time-domain electromagnetics on curvilinear domains: Int. J. Comput. Math., **88**, 2124–2153.

Gordon, W., and C. Hall, 1973, Transfinite element methods: Blending-function interpolation over arbitrary curved element domains: Numerische Mathematik, **21**, 109–129.

Hesthaven, J., and T. Warburton, 2007, Nodal discontinuous Galerkin methods: Algorithms, analysis, and applications: Springer. Texts in Applied Mathematics.

Käser, M., and M. Dumbser, 2006, An arbitrary high-order discontinuous Galerkin method for elastic waves on unstructured meshes I. the two-dimensional isotropic case with external source terms: Geophysical Journal International, **166**, 855–877.

Krivodonova, L., and M. Berger, 2006, High-order accurate implementation of solid wall boundary conditions in curved geometries: Journal of Computational Physics, **211**, 492 – 512.

Monk, P., and D.-Q. Wang, 1999, A least-squares method for the Helmholtz equation: Computer Methods in Applied Mechanics and Engineering, **175**, 121–136.

Reed, W., and T. Hill, 1973, Triangular mesh methods for the neutron transport equation: Los Alamos Scientic Laboratory Report, **LA-UR-73-479**.

Strang, G., and A. E. Berger, 1971, The change in solution due to change in domain: AMS Symposium on Partial Differential Equations, Berkeley, 199–206.

Symes, W., and T. Vdovina, 2009, Interface error analysis for numerical wave propagation: Computational Geosciences, **13**, 363–371.

Thomée, V., 1973, Polygonal domain approximation in Dirichlet's problem: IMA Journal of Applied Mathematics, **11**, 33–44.

Toulorge, T., Y. Reymen, and W. Desmet, 2008, A 2D discontinuous Galerkin method for aeroacoustics with curved boundary treatment, *in* Proceedings of International Conference on Noise and Vibration Engineering: 565–578.

Wang, X., 2010, Discontinuous Galerkin time domain methods for acoustics and comparison with finite difference time domain methods: Master's thesis, Rice University.

Warburton, T., 2013, A low-storage curvilinear discontinuous Galerkin method for wave problems: SIAM Journal on Scientific Computing, **35**, A1987–A2012.